Accelerated Publications

Mechanism of the *Escherichia coli* ADP-Ribose Pyrophosphatase, a Nudix Hydrolase[†,‡]

Sandra B. Gabelli,[§] Mario A. Bianchet,[§] Yuki Ohnishi,[∥] Yoshi Ichikawa,[⊥] Maurice J. Bessman,[@] and L. Mario Amzel*[,§]

Department of Biophysics and Biophysical Chemistry, School of Medicine, Johns Hopkins University, Baltimore, Maryland 21205, Optimer Pharmaceuticals, Inc., San Diego, California 92121, Department of Pharmacology, School of Medicine, Johns Hopkins University, Baltimore, Maryland 21205, and Department of Biology, McCollum-Pratt Institute, School of Arts and Sciences, Johns Hopkins University, Baltimore, Maryland 21218

Received April 5, 2002; Revised Manuscript Received May 29, 2002

ABSTRACT: *Escherichia coli* ADP-ribose (ADPR) pyrophosphatase (ADPRase), a Nudix enzyme, catalyzes the Mg^{2+}-dependent hydrolysis of ADP-ribose to AMP and ribose 5-phosphate. ADPR hydrolysis experiments conducted in the presence of $H_2{}^{18}O$ and analyzed by electrospray mass spectrometry showed that the ADPRase-catalyzed reaction takes place through nucleophilic attack at the adenosyl phosphate. The structure of ADPRase in complex with Mg^{2+} and a nonhydrolyzable ADPR analogue, α,*β*-methylene ADP-ribose, reveals an active site water molecule poised for nucleophilic attack on the adenosyl phosphate. This water molecule is activated by two magnesium ions, and its oxygen contacts the target phosphorus (P−O distance of 3.0 Å) and forms an angle of 177° with the scissile bond, suggesting an associative mechanism. A third Mg^{2+} ion bridges the two phosphates and could stabilize the negative charge of the leaving group, ribose 5-phosphate. The structure of the ternary complex also shows that loop L9 moves fully 10 Å from its position in the free enzyme, forming a tighter turn and bringing Glu 162 to its catalytic position. These observations indicate that as part of the catalytic mechanism, the ADPRase cycles between an open (free enzyme) and a closed (substrate−metal complex) conformation. This cycling may be important in preventing nonspecific hydrolysis of other nucleotides.

Nudix (nucleotide diphosphate X) pyrophosphatases, metal-requiring phosphoanhydrases that catalyze the hydrolysis of diphosphate linkages in nucleotide derivatives, are characterized by the presence of the signature sequence $GX_5EX_7REUXEEX_2U$ (*1*). They have been observed in species ranging from prokaryotes to eukaryotes; their postulated role is to clear the cell of toxic metabolites. One group, the Nudix ADP-ribose pyrophosphatases (ADPRases, Figure 1), catalyzes the hydrolysis of ADP ribose (ADPR), producing AMP and ribose 5-phosphate (R5P) (EC 3.1.6). At least two phenotypes have been associated with the expression of bacterial ADPRases: (1) tellurite (TeO_2, a toxic tellurium compound) resistance and (2) regulation of glycogen biosynthesis. In *Rhodobacter sphaeroides*, the TRGB gene, which encodes an ADPRase, is a tellurite resistance determinant (*2*). Also, transformation of *Escherichia coli* with a plasmid containing the *Methanococcus jannaschii* ADPRase gene dramatically increases the tellurite resistance of *E. coli* (*3*). In *E. coli*, an ADPRase (the product of the *yqiE* gene) controls glycogen biosynthesis by hydrolyzing its synthetic precursor, ADP glucose (*4*). Both of these functions, as well as the prevention of nonenzymatic ADP ribosylation of cellular proteins, fit well into the general role of Nudix pyrophosphatases as sanitizers of the cell (*1*).

The *E. coli* ADPRase is a homodimer with 209 amino acids per monomer. Its crystal structure (*5*) revealed that each monomer comprises two domains, an N-terminal domain and a Nudix fold domain common to all Nudix enzymes (*6*, *7*). The dimer is held together by extensive domain swapping such that each of the two substrate binding sites is formed by residues of both monomers. In contrast, each metal binding site is formed by residues of the Nudix signature sequence of a single monomer.

Preliminary mechanistic information about the *E. coli* ADPRase comes from two sources: the paper electrophoretic identification of the reaction products (*3*) and the crystallographic structures of the complexes of the enzyme with either metal or ADPR (*5*). Since the intrinsic activity of the

[†] This research was supported by Grants GM45540 (to L.M.A.) and GM18649 (to M.J.B.) from the NIGMS.

[‡] Coordinates of the structure have been deposited in the Protein Data Bank (entry 1KHZ).

* To whom correspondence should be addressed. Phone: (410) 955-3955. Fax: (410) 955-0637. E-mail: mario@neruda.med.jhmi.edu.

[§] Department of Biophysics and Biophysical Chemistry, School of Medicine, Johns Hopkins University.

[∥] Optimer Pharmaceuticals, Inc.

[⊥] Department of Pharmacology, School of Medicine, Johns Hopkins University.

[@] School of Arts and Sciences, Johns Hopkins University.

10.1021/bi0259296 CCC: $22.00
Published on Web 07/02/2002

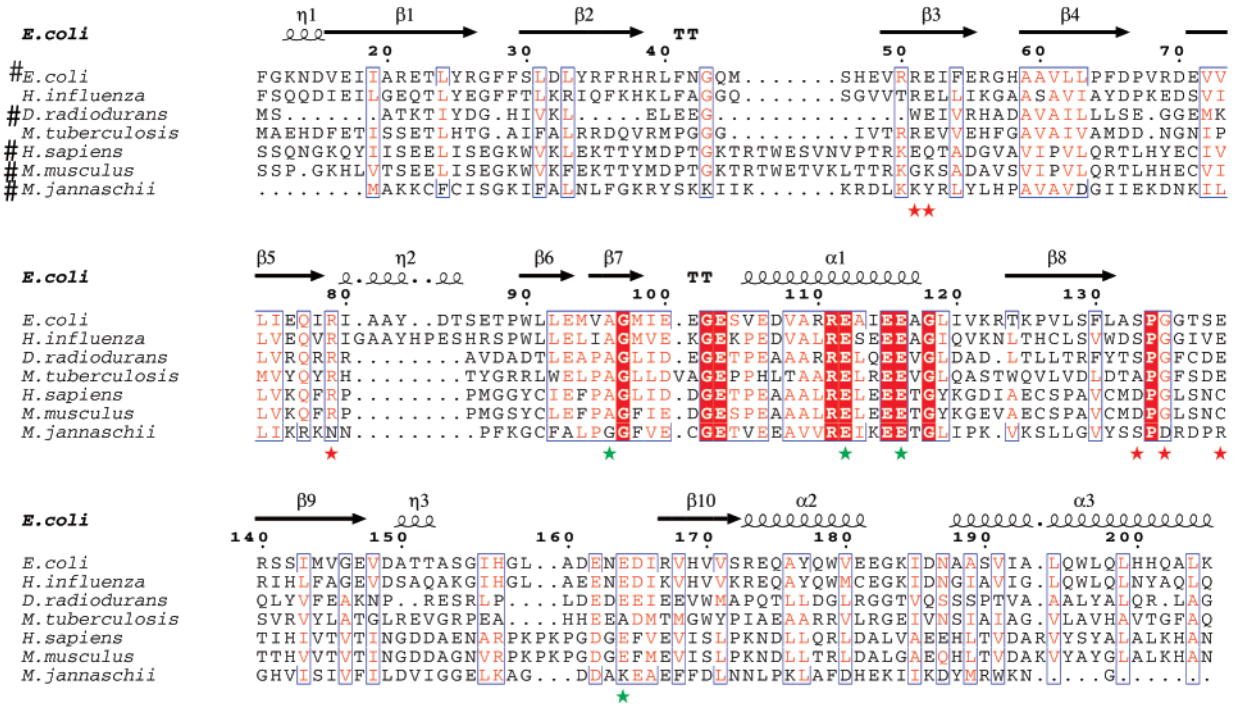

FIGURE 1: Alignment of ADPRase sequences. Enzymes that were characterized biochemically are marked with #. Secondary structural elements of the *E. coli* ADPRase (1G0S) are shown with coils (helices) and arrows (strands). Sequences shown here are as follows: (1) *E. coli* (EcORF209, P36651), (2) *Haemophilus influenzae* (Hi0398, P44684), (3) *Deinococcus radiodurans* (AAF10582), (4) *Mycobacterium tuberculosis* (Tb, O33199), (5) *Homo sapiens* (NUDT5, AF218818), (6) *Musculus musculus* (mNudT5, AF222786), and (7) *M. jannaschii* (Mj1149, Q58549). Areas of sequence similarity are boxed with a white background and areas of sequence identity boxed with red background. The alignment was prepared with Clustal X and ESPript. Red stars denote residues involved in substrate and/or inhibitor binding and green stars those involved in metal binding. The proposed catalytic base is residue 162 of the *E. coli* sequence.

ADPRase prevents the preparation and characterization of the enzyme−metal−ADPR complex, fundamental questions about the mechanism of the reaction remained unanswered: (1) Which of the two ADPR phosphates is the target of the nucleophilic attack? (2) What is the role of the metal(s)? (3) Which residue is the catalytic base that abstracts the proton from the attacking water? To answer the first question, we carried out catalytic hydrolysis of ADPR in $H_2{}^{18}O$ and analyzed the products using mass spectrometry. To answer the last two questions, we synthesized the nonhydrolyzable ADPR analogue α,*β*-methyleneadenosine diphosphoribose (AMPCPR) and determined the crystal structure of the ternary complex of *E. coli* ADPRase, magnesium, and AMPCPR.

EXPERIMENTAL PROCEDURES

Synthesis of an ADP Ribose Analogue. α,*β*-Methylene-ADP ribose was synthesized as described by Pankiewicz et al. (*8*). A stock solution (100 mM) was prepared in water and neutralized using NaHEPES.

Protein Expression, Purification, and Crystallization of the ADPRase. Overexpression, purification, and determination of enzymatic activity of the *E. coli* ADPRase were carried out as described previously (*3*). ADPRase in 50 mM Tris-HCl (pH 7.5) and 1 mM EDTA was crystallized using 10% PEG 1000 and 10% PEG 8000. For data collection, crystals were cryoprotected by adding a higher concentration of PEG as described previously (*5*).

Determination of the Structure of the Ternary Complex of AMPCPR and Mg^{2+} with ADPRase. Native crystals were soaked for 1 h in mother liquor containing 5 mM AMPCPR and 5 mM $MgCl_2$. Data to 2.07 Å resolution were collected on a CCD detector (Brandeis B4) at beamline X25 at NSLS, Brookhaven National Laboratory (Upton, NY). Diffraction data were processed with DENZO and SCALEPACK (*9*). An electron density map calculated with native phases showed well-resolved density that allowed fitting of all portions of the AMPCPR. Three peaks were identified as the Mg^{2+} ions because they showed octahedral coordination with Mg−O distances shorter than 2.3 Å. A model consisting of native coordinates, those of the inhibitor, and those of the metals was refined using the Crystallography & NMR System (CNS) (*10*) with a residual target that did not include noncrystallographic symmetry restraints. Rebuilding and correction of the model was guided by σA-corrected $2F_o - F_c$ electron density maps. R and R_{free} (calculated with a randomly selected 10% of the reflections) values were used to monitor refinement of the model (*11*). The final refinement and model statistics are shown in Table 1.

Determination of the Site of Nucleophilic Substitution by Electrospray Mass Spectrometry. A reaction mixture containing 50 mM Tris (pH 7.0), 5 mM $MgCl_2$, 1 mM dithiothreitol, 10 mM substrate, and 10 ng of ADP-ribose pyrophosphatase was prepared in a final volume of 50 μL using $H_2{}^{18}O$. Products of the reaction were analyzed on a QSTAR Pulsar quadrupole time-of-flight tandem mass spectrometer (Applied Biosystems/MDX Sciex, Foster City, CA). Samples were diluted to 30 μM in 50% methanol and 0.1% triethylamine and infused with a syringe pump at 5 μL/min. Spectra were obtained by scanning a mass range of 200−600 kDa in the negative mode with a −4.5 kV ion spray

Table 1: Crystallographic Data

data set	ADPRase−Mg^{2+}−AMPCPR
space group	$P2_12_12_1$
cell constants	$a = 67.1$ Å, $b = 67.4$ Å, $c = 96.5$ Å
resolution (Å)	40.0−2.07
no. of observed reflections	140757
no. of unique reflections	27868 (2791)
completeness (%)	94.0 (92.7)
R_{sym}	0.11 (0.24)
refinement	
R_{cryst}/R_{free}	0.19/0.25
model composition	
no. of amino acids	407
no. of metals	3 Mg^{2+}
no. of ligands	1 AMPCPR
no. of water molecules	225
no. of total atoms	3524
stereochemistry	
rms for bond lengths (Å)	0.012
rms for angles (deg)	1.85
⟨*B*-factor protein⟩ (Å^2)	22.8
⟨*B*-factor solvent⟩ (Å^2)	30.7
⟨*B*-factorAMPCPR⟩ (Å^2)	21.1

voltage and a 1 s accumulation time averaged over a 1 min duration.

Other Computations. The quality of the structures was assessed with the program PROCHECK (*12*). Buried areas were calculated with CNS (*10*) using a 1.4 Å probe. Figures were drawn with MOLSCRIPT (*13*), BOBSCRIPT (*14*), and RASTER3D (*15*). The sequence alignment was done with CLUSTALX (*16*), and the postscript figures were generated with ESPrit (*17*).

RESULTS AND DISCUSSION

Site of Nucleophilic Substitution

Since both phosphate groups of ADPR are bound to the 5′-position of a ribose, their intrinsic reactivities are essentially equivalent. The structure of the binary complex of ADPRase and ADPR provided no obvious clue as to whether hydrolysis of ADPR proceeded by nucleophilic attack at the adenosyl phosphate or at the ribosyl phosphate (*5*). To determine which phosphate is attacked, the enzymatic reaction was carried out in the presence of $H_2{}^{18}O$ and the products were analyzed by time-of-flight tandem mass spectrometry. The region of the spectrum corresponding to AMP (mass of 346) was highly enriched in ^{18}O, consistent with an attack on the adenosine phosphate. [The peak with a mass of 346 + 2 represented 66% of the molecules (Figure 2a). The limit of 66% enrichment is a consequence of the reaction conditions under which the protein was added in unlabeled water.] In contrast, the region of the ribose 5-phosphate has three peaks with masses of 229, 230, and 231 in the natural abundance proportions (Figure 2b), arguing against an attack at the ribosyl phosphate. These results establish that the nucleophilic attack by H_2O occurs at the phosphorus of the adenosyl phosphate.

Ternary Complex of ADPRase, AMPCPR, and Mg^{2+}

Structure Determination and Refinement. The apo-ADPRase crystals described earlier (*5*), soaked in mother liquor containing the substrate analogue AMPCPR and $MgCl_2$, remain isomorphous to the original crystals of the free enzyme and diffract to 2.07 Å resolution (Table 1). After refinement of the protein coordinates against this data set, $F_o - F_c$ and $2F_o - F_c$ maps showed clear electron density for one molecule of inhibitor and three magnesium ions (Mg1, Mg2, and Mg3) in one of the two catalytic sites (Figure 3a,b). Introduction of these compounds improved the refinement to a final R value of 19% ($R_{free} = 25\%$). At this stage, the $F_o - F_c$ map was completely featureless, including the region of the unoccupied catalytic site. After refinement with full occupancy, the average temperature factor of the AMPCPR molecule was 21.1 Å^2, and those of the three Mg^{2+} ions were 19.3, 22.5, and 19.5 Å^2, respectively, all slightly lower than the average of the protein atoms.

Differences between Monomers. In the crystals of the ternary complex, the two monomers in the asymmetric unit differ in several respects. As mentioned above, only one of the two catalytic sites is occupied, probably as a result of packing differences between the two monomers. This results

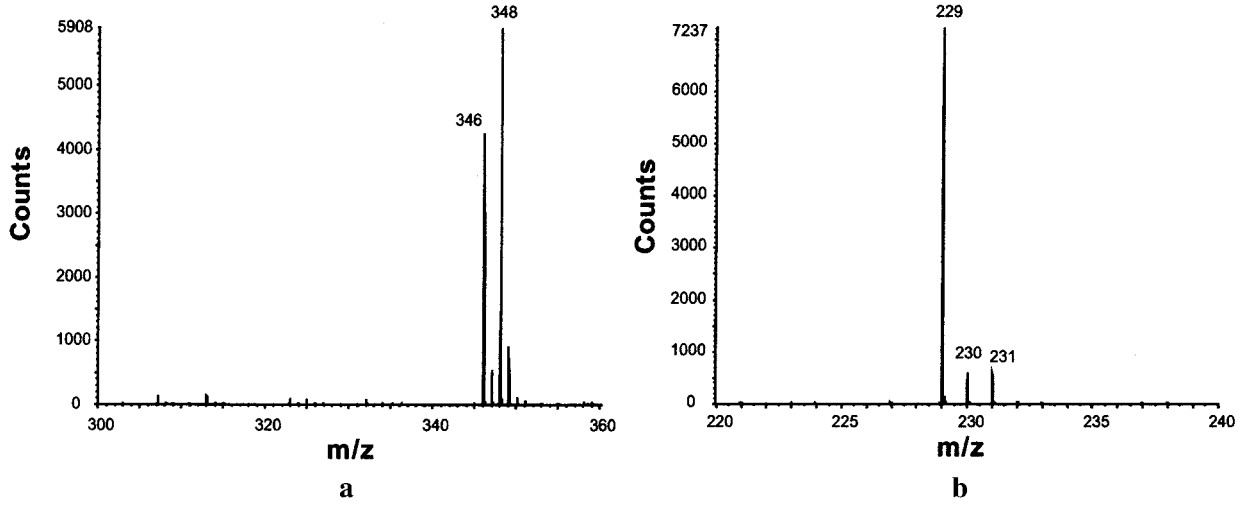

FIGURE 2: Negative ion electrospray mass spectra of ADPRase reaction products. Analysis of the products of ADP ribose hydrolysis in $H_2{}^{18}O$ in the presence of purified ADPRase with 5 mM ADP ribose at 37 °C for 15 min in 50 mM Tris-HCl (pH 7) and 5 mM Mg^{2+}. Spectra of a reaction mixture after hydrolysis by ADPRase in $H_2{}^{18}O$: (a) a mass of 348 (346 + 2) corresponds to labeled AMP (mass of 346) and (b) a mass of 229 corresponds to unlabeled ribose 5-phosphate. ADPRase transfers ^{18}O from $H_2{}^{18}O$ to AMP. Mass spectrometric conditions are described in Experimental Procedures.

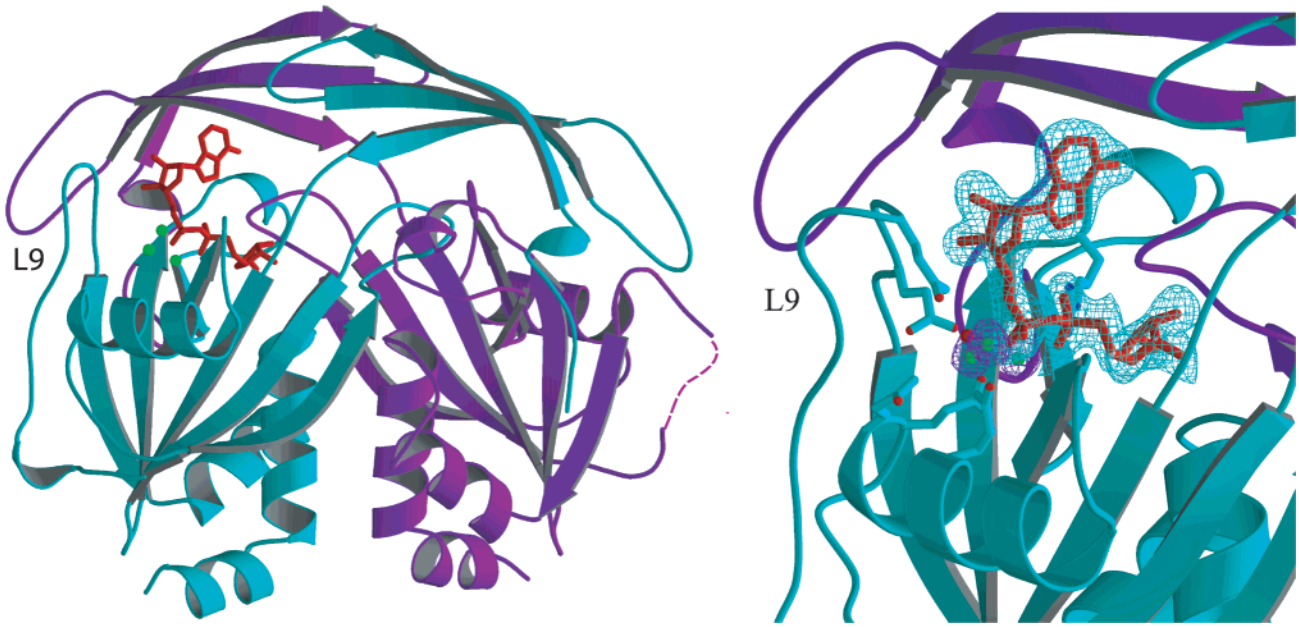

FIGURE 3: (a) Ribbon diagram of the ADPRase in complex with the trinuclear Mg^{2+} cluster and AMPCPR. (b) The $2F_o - F_c$ electron density of the AMPCPR and the magnesium ions. The density of the AMPCPR is shown in turquoise and that of the Mg^{2+} ions in purple.

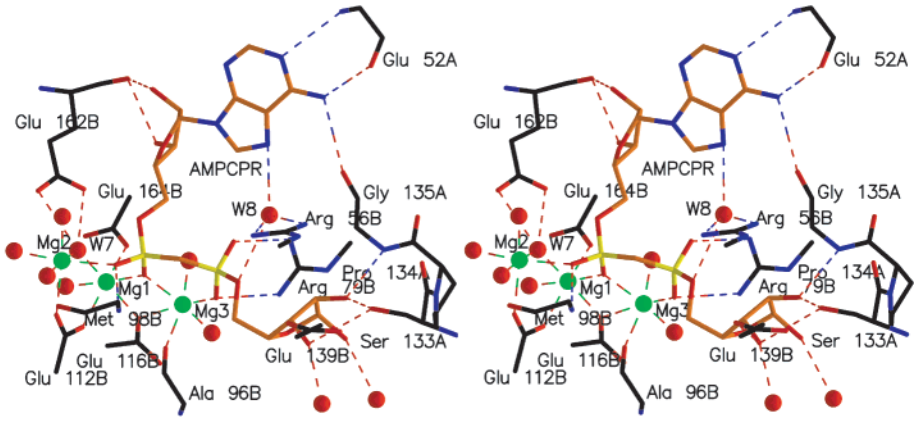

FIGURE 4: Stereodiagram of the interactions of the AMPCPR and the Mg^{2+} ions with ADPRase. All H-bonds are represented with dashed lines. A and B indicate the monomer to which the residue belongs. Carbon atoms are orange in the inhibitor and black in the protein; nitrogens are blue, phosphorus yellow, and oxygens red. Water molecules are shown as red spheres; magnesium ions are shown as green spheres.

in major differences in one of the loops that forms the catalytic site. In the monomer with the unoccupied site, loop L9, spanning residues 155−167, is disordered and was not included in the final model. In the monomer with the occupied binding site, the same loop is well-defined and participates in binding the substrate analogue (see below).

Binding of AMPCPR. Both monomers, A and B, contribute to the binding of the AMPCPR to this site on the enzyme. Residues belonging to the monomer providing the Nudix motif are labeled B, and those from the other monomer are labeled A. The AMPCPR is held in a horseshoe conformation, similar to that observed for ADPR in the binary complex (*5*), by hydrogen bonds from adenine N7 and the ribosyl phosphate oxygen to the same water molecule, W8 (Figure 4). Arg 56B also makes a hydrogen bond to water molecule W8. Hydrogen bonds between N6 and the carbonyl oxygens of Glu 52A and Gly 135A and a hydrogen bond between N1 and the amide nitrogen of Glu 52A provide the major interactions with the adenine base. In addition, the carbonyl of Glu 162B makes a hydrogen bond with oxygen AO2 of the adenyl ribose. The terminal ribose is hydrogen bonded to Ser 133A and Glu 139B. The nucleoside conformation is highly similar to that of the ADPR in the binary complex. The AMPCPR has a glycosidic torsion angle of −155°, with C3-endo puckering in the adenosyl ribose and C2-endo puckering in the ribosyl sugar. The second active site is empty, and its corresponding loop L9 (residues 155−166) is disordered, as was observed in the native, metal-bound, and substrate-bound structures. Interestingly, the disordered loop includes Glu 164B, a metal ligand, and Glu 162B, the catalytic base (see below). Although this half-occupancy might argue in favor of half-of-the-sites reactivity, the interaction of the unoccupied site with a neighboring molecule in the crystal provides an alternative explanation. As a result of this contact, residues Glu 17 and Ile 19 of the neighboring molecule partially occlude the binding site, and loop L9 of the unoccupied monomer may be prevented from carrying out the movement required for binding of metal and the substrate analogue. Binding of substrate in the absence of metal has been observed in the structure of the binary

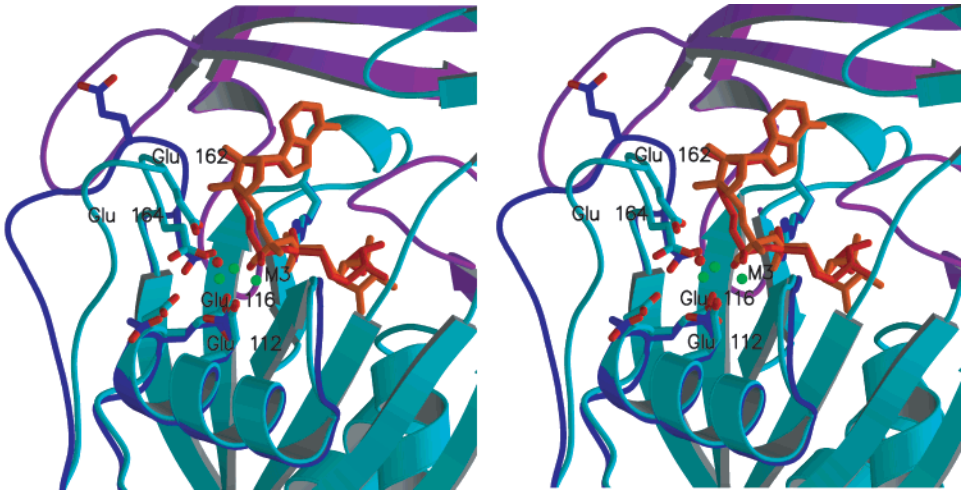

FIGURE 5: Stereodiagram of the overlap of the binary and ternary complex of the ADPRase. Closeup of the active site showing the trinuclear Mg^{2+} cluster and the position of Glu 162 in the open and closed conformations. The structure of the main chain of the binary complex is shown in dark blue and that of the ternary complex in light blue. Loop L9 is the only major structure element that moves. Atoms of the inhibitor are orange and those of the substrate red; side chain carbon atoms are colored either dark blue (binary complex) or light blue (ternary complex), and side chain oxygens are colored red. Water molecules are shown as red spheres; magnesium ions are shown as green spheres.

complex (*5*), even in the presence of partial occlusion and without the conformational change of loop L9. Why then is the empty site not occupied by AMPCPR without metal? The most likely explanation is that, given the concentrations of AMPCPR and Mg^{2+} (5 mM each), the substrate analogue exists predominantly as the Mg^{2+} complex so that free AMPCPR is not available to occupy the empty site.

Coordination of Mg^{2+} Ions. The three magnesium ions bound to ADPRase in the ternary complex form a trinuclear cluster in which two ions are 3.5 and 3.2 Å from a central ion, Mg1 (Figures 3b and 4). The distances between the magnesium ions are consistent with those observed in other binuclear and trinuclear magnesium and manganese clusters (*18*). The three ions are octahedrally coordinated entirely by oxygen ligands with an average Mg−O distance of 2.2 Å, as expected for octahedral Mg^{2+} coordination by oxygen atoms (*19*). Mg1 is coordinated with nearly perfect octahedral geometry by one oxygen atom from each of the following groups: the carboxylates of Glu 112, Glu 116, and Glu 164, the adenosyl phosphate, and two water molecules (Figure 4). The ligands of Mg2 include one oxygen atom of the Glu 112 carboxylate, one oxygen atom of the adenosyl phosphate, and four water molecules. Mg3 is coordinated by oxygen atoms of the adenosyl and ribosyl phosphates, by a carboxylate oxygen of Glu 116 (one of the strictly conserved residues of the Nudix signature sequence), and by the main chain carbonyl oxygen of Ala 96. Water molecule W7, coordinated to both Mg1 and Mg2, is in line with the scissile bond (the O−P−O angle is 177°).

Comparison of the Binary and Ternary Complexes

Comparison of the structure of the binary complex (ADPRase with ADPR) with that of the ternary complex (ADPRase with AMPCPR and the trinuclear magnesium cluster) shows an rms deviation of only 0.5 Å for α-carbons. The secondary structure elements are the same in both structures and show excellent alignment. Significantly, the two dimers differ only in the position of loop L9 of the monomers that contains the inhibitor molecule in the ternary complex. The average translation for residues 155−167 is 5 Å, with a maximum displacement of 10 Å in the region that includes Asp 161 and Glu 162. This movement of loop L9 of the occupied site toward the metal binding site brings Glu 162 to a position where it can act as the catalytic base (Figure 5). A similar conformational change induced by a substrate analogue with metal binding has been observed in 5′-nucleotidases (*20*).

The conformational change tightens loop L9 and allows the formation of six new main chain−main chain hydrogen bonds. These hydrogen bonds and the interaction of Glu 162 with water molecule W7 stabilize the new conformation of the loop.

Many of the hydrogen bonds involved in the recognition of the substrate and/or inhibitor are common to the binary complex and ternary complex, but the movement of loop L9 and other small rearrangements within the binding site maximize the hydrogen bonds between AMPCPR and the protein in the ternary complex. The most important change in the hydrogen bonding pattern is the shift of the interaction of the adenosyl ribose from the main chain carbonyl of Asn 163B to the carbonyl of Glu 162B. This altered H-bond may help position Glu 162B to act as the catalytic base.

The molecular surface of the ADPRase calculated in the presence of the substrate ADPR suggests an open binding site with a negatively charged floor corresponding to the region of the carboxylate cluster of the Nudix signature sequence (Figure 7). In contrast, the molecular surface of the ternary complex structure (calculated in the presence of magnesium and the inhibitor) shows that the same area of the binding site has become positively charged and therefore more favorable for binding the substrates' phosphates (Figure 7). This change in polarity is due in part to the presence of the three Mg^{2+} ions.

Mechanism

Hydrolysis of ADPR catalyzed by ADPRase in the presence of $H_2{}^{18}O$ showed that the reaction proceeds via a nucleophilic attack on the adenosyl phosphate. The structure

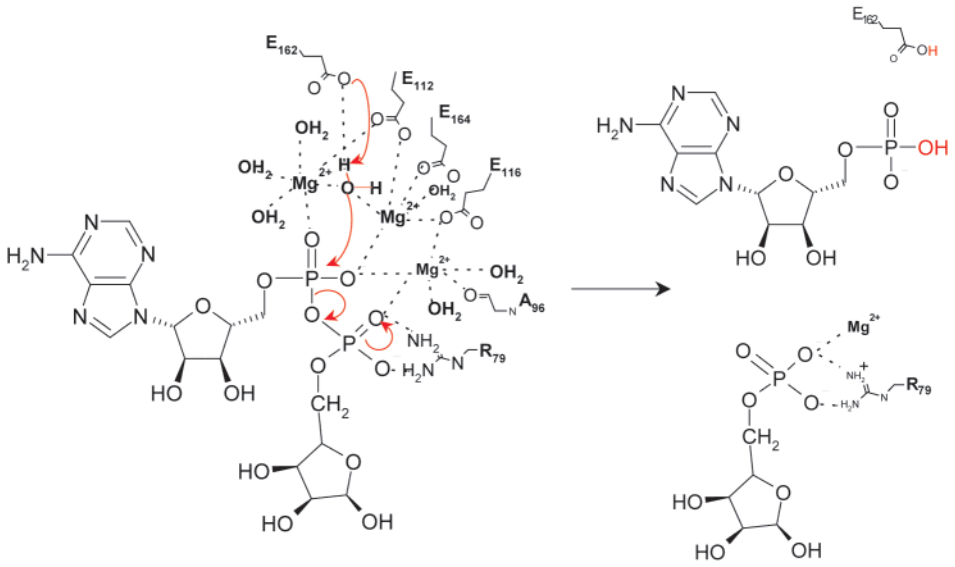

FIGURE 6: Mechanism for *E. coli* ADPRase based on the structure of the ternary complex and the mass spectrometry data. A water molecule is the nucleophile that attacks the adenosyl phophorus. This water molecule coordinates two Mg^{2+} ions and is only 3 Å from the phosphorus of the adenosyl phosphate. Glu 162 is positioned by the movement of loop L9 to act as the catalytic base.

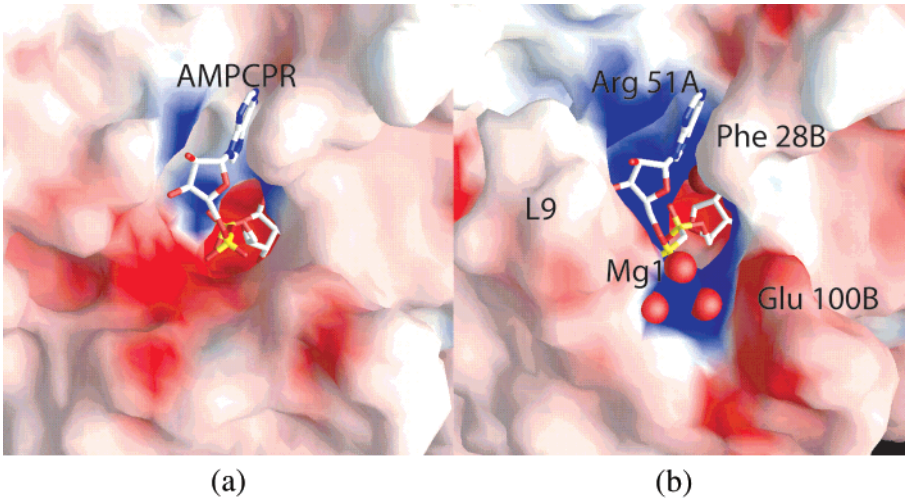

FIGURE 7: Electrostatic potential at the binding site mapped onto the molecular surface of the ADPRase dimer. Red is negative (−19 kT), and blue is positive (+19 kT). The picture was prepared with GRASP (*22*). (a) ADPRase with bound ADPR. The bottom of the cavity shows a negative surface that is compensated upon binding of Mg^{2+} ions (see panel b). Water molecules are shown as red spheres. (b) ADPRase with bound AMPCPR and Mg^{2+}. Loop L9 moves to close up the binding site.

of the ternary complex of ADPRase with the nonhydrolyzable substrate analogue AMPCPR and the trinuclear magnesium cluster also shows that the attacking water molecule (W7) is activated by bridging two Mg^{2+} ions and is in a favorable position for the nucleophilic attack, with its oxygen contacting the phosphorus (3.0 Å) and forming an angle (water−phosphorus−bridging oxygen) of 177°, consistent with an associative mechanism. The third Mg^{2+} ion bridges the two phosphates and may help stabilize the charge of the leaving group, ribose 5-phosphate. Arg 79A of the other monomer, which makes hydrogen bonds to the ribosyl phosphate group, stabilizes the negative charge on the ribose 5-phosphate in the ternary complex (Figure 6). Comparison of the structures of the apoenzyme and the ternary complex shows that binding of substrate in the presence of activating concentrations of Mg^{2+} results in a change in the conformation of loop L9 that closes the catalytic site and brings Glu 162B to a location where it is ideally positioned to act as the catalytic base. Thus, during catalysis the enzyme cycles between two conformations: open, after release of products, and closed, while the reactants and the transition state are bound to the enzyme.

In the proposed mechanism, Glu 162B carries out the proton abstraction as part of the hydrolytic reaction. Since the attacking water molecule, W7, bridges Mg1 and Mg2, its pK_a must be lowered, making it a better nucleophile, or even allowing it to lose a proton before it attacks the phosphate. Thus, deprotonation by Glu 162B can occur either as part of the attack on the adenosyl phosphate or as the water binds to the two magnesium ions, binding as a hydroxyl. Nucleophilic attacks by hydroxide ions have been proposed in other binuclear and trinuclear metal centers (*21*).

On the basis of the conservation of the Nudix signature sequence as well as of key amino acids involved in substrate recognition and catalysis, we propose that this catalytic mechanism is common to all Nudix ADPRases. Except for these amino acids, ADPRases display a low level of identity among different species (Figure 1).

Structural Implications for Other ADPRases

Nudix APDRases are ubiquitous enzymes present in all three kingdoms. Alignment of their sequences shows, in addition to the conserved residues of the Nudix signature sequence, a position 16 residues downstream from this sequence that is characteristic of the different Nudix subfamilies. In ADPRases, this position is occupied by a proline, Pro 134 in *E. coli* (Figure 1), that promotes a tight bend. This bend positions two residues, Ser 133 and Gly 135, that make H-bonds to the terminal ribose. The structure presented here shows that additional highly conserved residues within bacterial ADPRases are involved in substrate recognition (Figure 1). These residues, conserved within the bacterial enzymes, include Arg 51 which is stacked against the adenosine base, Glu 52 which is at hydrogen bonding distance of N1 and N6 of the adenine ring, Arg 79 NH1 and NH2 which are at hydrogen bonding distance from the oxygen atoms of the ribosyl phosphate, Gly 135 which is at hydrogen bonding distance from adenine and the oxygen of the terminal ribose, and Glu 139 which is at hydrogen bonding distance from O2 of the terminal ribose. The sequence position corresponding to the catalytic base, Glu 162, not only is more than 70% identical among all sequences but also is part of a region rich in carboxylates that could provide other residues as catalytic bases depending on the conformation and length of loop L9. The only two metal ligands that lie outside the Nudix signature sequence, Ala 96 and Glu 164, are absolutely conserved among bacterial enzymes and display a high level of conservation in all species. The identity of the binding site residues of both monomers suggests that domain swapping is also conserved among species.

SUMMARY

The data presented here provide definite answers to key questions concerning the mechanism of *E. coli* ADPRase. In this mechanism, the free enzyme is in the open conformation. Binding of substrate and Mg^{2+} promotes a conformational change that repositions several residues, including the catalytic base. The need for this conformational change may add to the selectivity of the enzyme: only substrates that trigger the change can be hydrolyzed.

In the closed conformation, the attacking water molecule is coordinated to two Mg^{2+} ions that lower its pK_a and make it a better nucleophile. Attack occurs at the adenosine phosphate, and the charge in the leaving ribose 5-phosphate is neutralized by a third Mg^{2+} ion, as well as an arginine residue. Conservation of active site residues and of amino acids involved in substrate specificity suggests that all Nudix ADPRases utilize a similar mechanism.

ACKNOWLEDGMENT

Some of the data were collected at the National Synchrotron Light Source, Brookhaven National Laboratory, which is supported by the U.S. Department of Energy, Division of Materials Sciences and Division of Chemical Sciences. Mass spectrometry was carried out at the mass spectrometry facility at Johns Hopkins Medical Institutions by R. Cole. We thank Drs. Dan Leahy and Jon Lorsch for carefully reading the manuscript.

REFERENCES

1. Bessman, M. J., Frick, D. N., and O'Handley, S. F. (1996) *J. Biol. Chem. 271*, 25059−25062.
2. O'Gara, J. P., Gomelsky, M., and Kaplan, S. (1997) *Appl. Environ. Microbiol. 63*, 4713−4720.
3. Dunn, C. A., O'Handley, S. F., Frick, D. N., and Bessman, M. J. (1999) *J. Biol. Chem. 274*, 32318−32324.
4. Moreno-Bruna, B., Baroja-Fernandez, E., Munoz, F. J., Bastarrica-Berasategui, A., Zandueta-Criado, A., Rodriguez-Lopez, M., Lasa, I., Akazawa, T., and Pozueta-Romero, J. (2001) *Proc. Natl. Acad. Sci. U.S.A. 98*, 8128−8132.
5. Gabelli, S. B., Bianchet, M. A., Bessman, M. J., and Amzel, L. M. (2001) *Nat. Struct. Biol. 8*, 467−472.
6. Swarbrick, J., Bashtannyk, T., Maksel, D., Zhang, X., Blackburn, G., Gayler, K., and Gooley, P. (2000) *J. Mol. Biol. 302*, 1165−1177.
7. Abeygunawardana, C., Weber, D. J., Gittis, A. G., Frick, D. N., Lin, J., Miller, A. F., Bessman, M. J., and Mildvan, A. S. (1995) *Biochemistry 34*, 14997−15005.
8. Pankiewicz, K., Lesiak, K., and Watanabe, K. (1997) *J. Am. Chem. Soc. 119*, 3691−3695.
9. Otwinowski, Z., and Minor, W. (1997) *Methods Enzymol. 277*, 307−326.
10. Brunger, A. T., Adams, P. D., Clore, G. M., DeLano, W. L., Gros, P., Grosse-Kunstleve, R. W., Jiang, J., Kuszewski, J., Nilges, M., Pannu, N. S., Read, R., Rice, L., Simonson, T., and Warren, G. L. (1998) *Acta Crystallogr. D54*, 905−921.
11. Brunger, A. T. (1997) *Methods Enzymol. 277*, 366−396.
12. Laskowski, R., MacArthur, M., Moss, D., and Thornton, J. (1993) *J. Appl. Crystallogr. 26*, 283−291.
13. Kraulis, J. (1991) *J. Appl. Crystallogr. 24*, 946−950.
14. Esnouf, R. M. (1999) *Acta Crystallogr. D55*, 938−940.
15. Merrit, E., and Bacon, D. (1997) *Methods Enzymol. 277*, 505−524.
16. Thompson, J. D., Higgings, D. G., and Gibson, T. J. (1994) *Nucleic Acids Res. 22*, 4673−4680.
17. Gouet, P., Courcelle, E., Stuart, D. I., and Metoz, F. (1999) *Bioinformatics 15*, 305−308.
18. Wilce, M. C., Bond, C. S., Dixon, N. E., Freeman, H. C., Guss, J. M., Lilley, P. E., and Wilce, J. A. (1998) *Proc. Natl. Acad. Sci. U.S.A. 95*, 3472−3477.
19. Glusker, J. P. (1991) *Adv. Protein Chem. 42*, 1−77.
20. Strater, N., and Knotel, T. (2001) *J. Mol. Biol. 309*, 239−254.
21. Cox, J. D., Cama, E., Colleluori, D. M., Pethe, S., Boucher, J. L., Mansuy, D., Ash, D. E., and Christianson, D. W. (2001) *Biochemistry 40*, 2689−2701.
22. Nicholls, A., Sharp, K., and Honig, B. (1991) *Proteins: Struct., Funct., Genet. 11*, 281−296.

BI0259296